

Damage detection for beam structures using an angle-between-string-and-horizon flexibility matrix

Guirong Yan^{1a}, Zhongdong Duan^{*2} and Jinping Ou^{3,4b}

¹School of Engineering, University of Western Sydney, Penrith, NSW, 1797, Australia

²Shenzhen Graduate School, Harbin Institute of Technology, Shenzhen, 518055, China

³School of Civil and Hydraulic Engineering, Dalian University of Technology, Dalian, 116024, China

⁴School of Civil Engineering, Harbin Institute of Technology, Harbin, 150090, China

(Received July 24, 2008, Accepted August 19, 2010)

Abstract. The classical flexibility difference method detects damage by observing the difference of conventional deflection flexibility matrices between pre- and post-damaged states of a structure. This method is not able to identify multiple damage scenarios, and its criteria to identify damage depend upon the boundary conditions of structures. The key point behind the inability and dependence is revealed in this study. A more feasible flexibility for damage detection, the Angle-between-String-and-Horizon (ASH) flexibility, is proposed. The physical meaning of the new flexibility is given, and synthesis of the new flexibility matrix by modal frequencies and translational mode shapes is formulated. The damage indicators are extracted from the difference of ASH flexibility matrices between the pre- and post-damaged structures. One feature of the ASH flexibility is that the components in the ASH flexibility matrix are associated with elements instead of Nodes or DOFs. Therefore, the damage indicators based on the ASH flexibility are mapped to structural elements directly, and thus they can pinpoint the damaged elements, which is appealing to damage detection for complex structures. In addition, the change in the ASH flexibility caused by damage is not affected by boundary conditions, which simplifies the criteria to identify damage. Moreover, the proposed method can determine relatively the damage severity. Because the proposed damage indicator of an element mainly reflects the deflection change within the element itself, which significantly reduces the influence of the damage in one element on the damage indicators of other damaged elements, the proposed method can identify multiple damage locations. The viability of the proposed approach has been demonstrated by numerical examples and experimental tests on a cantilever beam and a simply supported beam.

Keywords: flexibility; angle-between-string-and-horizon flexibility; damage detection.

1. Introduction

Structural health monitoring and damage detection is important to maintain safety and integrity of structures, to increase their life span, and to reduce total life-cycle maintenance costs. Recent catastrophic failures of bridges around the world (for example, the I-35W highway bridge over the

*Corresponding author, Professor, E-mail: duanzd@hit.edu.cn

^aLecturer, E-mail: g.yan@uws.edu.au

^bProfessor, E-mail: oujinpings@dlut.edu.cn, oujinpings@hit.edu.cn

Mississippi River in Minneapolis, Minnesota, US 2007) underscore the need to develop an effective, fast, automatic and cost-effective structural health monitoring and damage detection system. To this end, vibration-based damage detection methods play an important role. Significant efforts have been dedicated in this field.

A lot of studies are based on frequency domain data obtained from modal analysis of vibration data. Some of them detect damage by investigating changes in extracted dynamic characteristics, such as natural frequencies, mode shapes, damping ratios or their derivatives (such as curvature mode shapes, strain mode shapes, frequency response function or flexibility matrices). The key point of this kind of methods is to find the dynamic characteristics which are sensitive to damage, and insensitive to measurement noises and variant measurement environment (Harri *et al.* 2008). Other methods localize and quantify damage by modifying structural finite element models using model updating techniques (Unger *et al.* 2006). A comprehensive literature review associated with these methods can be found in Doebling *et al.* (1996).

Some methods are based on time domain analysis. To detect damage online, Yang *et al.* (2006) employed the extended Kalman filter approach to identify structural parameters and tracked the changes of system parameters caused by damage. Yang *et al.* (2007) also proposed a recursive least-squares estimation with unknown inputs to identify structural parameters and the unmeasured excitations. Sakellariou and Fassois (2006) identified model parameters by minimizing the output error of the ARX model. Statistical hypothesis testing procedures were used for damage detection, and a geometric method was used for damage assessment.

Due to the fact that wavelet transform (WT) is capable of detecting singularity, removing noise from data, and providing the information on both time/location and frequency domains, damage detection based on WT has been well studied (Huang *et al.* 2009, Pakrashi *et al.* 2007, Law *et al.* 2005). For example, Basu (2005) employed the time-frequency characteristics extracted by WT to detect the system degradation. To make full use of the information in the time, frequency and space domains, a method based on the residual force extracted using WT was proposed. This method can determine both the damage sites and the time instants when the damage occurs (Yan *et al.* 2009).

Methods based on other theories have also been developed, such as neural network (Lee *et al.* 2005), fuzzy clustering (da Silva *et al.* 2008), sensitivity analysis of dynamic response (Lua and Law 2007), generalized minimum rank perturbation theory (D'Souza and Epureanu 2008), proper orthogonal decomposition (Galvanetto and Violaris 2007), information fusion technique (Guo 2006), and empirical mode decomposition (Li *et al.* 2007). Some advanced measurement techniques have been applied to improve damage detection results. For instance, a high speed digital video camera used to measure structural displacement response (Poudel *et al.* 2005), a laser Doppler vibrometer (LDV) used in a modal test (Siringoringo *et al.* 2006) and a wireless sensor network (Yan *et al.* 2010).

Among these methods, techniques for damage detection based on structural flexibility have been gaining much importance due to the two unique features of flexibility. First, the flexibility matrix is dominated by low-frequency modes, and thus a good estimation of flexibility can be obtained easily; second, the flexibility matrix at the measurement sensor coordinates can be extracted from the matrices of system realization. Research on how to construct structural flexibility from measured data has been conducted by Doebling and Peterson (1997), and Doebling and Farrar (1996).

Using numerical examples of different types of beams and experimental tests on a free-free beam, Pandey and Biswas (1994, 1995) demonstrated that the change in structural flexibility between the pre- and post-damaged states could be used to localize damage in beam-type structures. This

method is referred as “the classical flexibility difference method” in the sequel. However, this method has the following disadvantages. First, for beam structures with a free boundary condition, this method fails to localize multiple damage locations. Second, the change in structural flexibility is affected by support conditions, and thus the information on the boundary conditions of structures and the criterion to identify damage for each type of boundary condition should be available in advance.

In addition, because the classical flexibility difference method is based on the conventional deflection flexibility, damage detection results obtained are manifested as a nodal or DOF's (Degree Of Freedom) characterization. Therefore, this method is difficult to localize damage in structures which have load-path redundancy. It seems more reasonable to detect damage using localized flexibility by projecting damage on elements or substructures. Central to this type of methods is to decompose the global flexibility into localized sub-structural flexibility or elemental flexibility. Doebling and Peterson (1998) extracted sub-structural flexibility from the measured flexibility by projecting the experimentally measured flexibility matrix onto the strain energy distribution in local elements or regional super-elements, while Park *et al.* (1997) accomplished it through a complete variational decomposition of the energy functional of the dynamic system. Aoki and Byon (2001) employed similar algorithm to detect damage occurring inside CFRP filament winding pipes. However, using modal test data measured on an aircraft fuselage skin, Robinson and Peterson (1996) demonstrated that the results obtained using the conventional flexibility were better than the disassembled elemental flexibility. The Damage Location Vectors (DLVs) approach developed by Bernal and Gunes (2004) also has the ability to map changes in the measured flexibility to elements in a structure. Bernal (2002) and Duan *et al.* (2005) generalized the DLV method to the case of ambient vibration by using proportional flexibility matrices extracted by two different algorithms, respectively.

The objective of the work reported here is to develop a flexibility-based method for localizing and quantifying damage occurring in structures, which tries to avoid the difficulties faced by the methods developed before. Specifically, the method should be able to directly project damage onto elements or super-elements instead of nodes or DOFs, and thus it can localize damage to exact elements. Moreover, the method should be suitable for multiple damage cases and provide information on the damage extent. To meet this objective, a more feasible flexibility for damage detection, the Angle-between-String-and-Horizon (ASH) flexibility, is defined, and a damage detection method based on the ASH flexibility is developed. The effectiveness of the proposed damage detection method is validated by numerical simulations and experimental tests of beams with different support conditions.

2. The classical flexibility difference method based on deflection flexibility

Based on the fact that the presence of damage in structures reduces structural stiffness, and hence increases structural flexibility, the change in structural flexibility between the pre- and post-damaged states can be used to detect damage. The change in flexibility \mathbf{F} can be computed as

$$\Delta\mathbf{F} = \mathbf{F}^d - \mathbf{F}^u \quad (1)$$

where the superscripts d and u indicate the damaged and undamaged structures, respectively.

Deflection flexibility matrices are employed in Eq. (1), and they can be assembled by modal parameters as follows

$$\mathbf{F} = \mathbf{\Phi}\mathbf{\Omega}^{-1}\mathbf{\Phi}^T = \sum_{r=1}^n \frac{1}{\omega_r^2} \boldsymbol{\varphi}_r \boldsymbol{\varphi}_r^T \quad (2)$$

where $\boldsymbol{\varphi}_r$ is the r th mass-normalized mode shape, and $\mathbf{\Phi}$ is the mode shape matrix; ω_r is the r th circular modal frequency, and $\mathbf{\Omega}$ is the diagonal eigenvalue matrix with squares of ω_r ($r = 1, \dots, n$) as its diagonals; n is the number of modes used.

For a restrained structure, the components in the i th column of \mathbf{F} are the displacements at all DOFs resulting from a unit force applied at the i th DOF. As can be seen from Eq. (2), the contribution of a mode to \mathbf{F} decreases as the mode order increases. Therefore, a good estimate of the flexibility matrix can be obtained with easily identified low-frequency modes, which is appealing to civil engineering applications.

The diagonals or the maximum absolute values of the components in each column of $\Delta\mathbf{F}$ are extracted to form a vector of damage indicators, which are termed as $\delta\mathbf{F}d$ or $\delta\mathbf{F}m$, respectively. From $\delta\mathbf{F}d$ or $\delta\mathbf{F}m$, damage locations can be determined. It is worth noting that the change in the conventional deflection flexibility is affected by structural boundary conditions. For a cantilever beam, damage is localized by the node from which $\delta\mathbf{F}d$ or $\delta\mathbf{F}m$ starts to deviate from zero and grows gradually. For a simply supported beam, damage is localized by the nodes associated with maximum values in $\delta\mathbf{F}d$ or $\delta\mathbf{F}m$. Therefore, this method requires information on the boundary conditions of structures, and requires that users be familiar with the criteria to identify and localize damage for each type of boundary condition.

Apart from the above limitation, this method fails to localize multiple damage sites in some structures. An example of a cantilever beam is given here to try to disclose the reason of this failure. Its finite element model is shown in Fig. 1. Herein, normal and bold numbers indicate node numberings, and italic and bold numbers indicate element numberings. Damage is simulated in this example as a 50% reduction in the stiffness of Elements i and k . The damage in Element i results in an increase in the deflection of each node to the right of Element i , comparing with that of the intact structure, when a unit force is applied at one of these nodes which are located to the right of Node i . Therefore, we can identify the damage of Element i , which is close to the clamped end, by observing the location of the element in $\delta\mathbf{F}d$ or $\delta\mathbf{F}m$ that starts to deviate from zero, as shown in Fig. 2.

Now let us analyze why the other damage site (Element k) cannot be identified. The increase in deflection at each node to the right of Element k consists of two contributing factors: one is from the increase of deflection at the right node of Element k , and the other is from the increase of rotation at the right node of Element i . The increase of rotation results in the linear increase in the deflection at the nodes to the right of Element i , and this deflection increase at each node is proportional to the distance of this node from Element i . It is this rotation-related deflection increase caused by Element i in the left that masks any deflection increase caused by other damaged

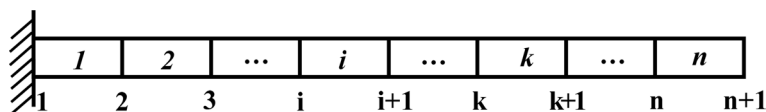


Fig. 1 A cantilever beam with discrete elements

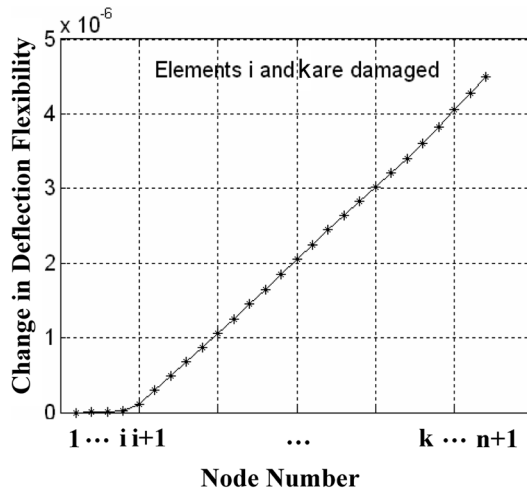


Fig. 2 The damage localization results using the deflection flexibility difference method

elements in the right (here, Element k). That’s why the other damaged element, Element k , cannot be identified in the plot of flexibility change versus number of DOFs, as shown in Fig. 2. Using the numerical analysis of a cantilever beam with seven elements, Appendix 1 demonstrates how the damage in the left which is closer to the clamped end affects the damage indicators (based on the conventional deflection flexibility) of the following nodes.

3. The angle-between-string-and-horizon flexibility matrix

In this section, a more feasible flexibility for damage detection, which is called the Angle-between-String-and-Horizon (ASH) flexibility, is defined for beam-type structures. The components in the i th column of this flexibility matrix represent the ASHs of all elements resulting from a unit moment applied at the two nodes of Element i (as a couple with opposing forces applied at the two end nodes of Element i), and no force or moment on the other elements. Take a cantilever beam with n elements (shown in Fig. 1) as an example, the formulation of the ASH flexibility in terms of translational modes is derived as follows.

To obtain the i th column of the ASH flexibility, a unit moment is applied at the two nodes of Element i (Nodes i and $i+1$). As the definition indicated, this unit moment is applied as a pair of parallel forces with equal amplitudes but opposite directions at the two nodes of Element i , respectively. The amplitudes of the forces are $1/l_i$, where l_i is the length of Element i . On the other hand, the ASH of one element can be reflected by the relative displacement (in the vertical direction) per unit length of this element between its two nodes, which is equal to the displacement difference between its two nodes divided by the length of this element. Therefore, based on the superimposition of loads shown in Fig. 3 and the physical significance of conventional deflection flexibility, the ASH of Element k (the k th component in the i th column of the ASH flexibility) resulting from this unit moment can be obtained as

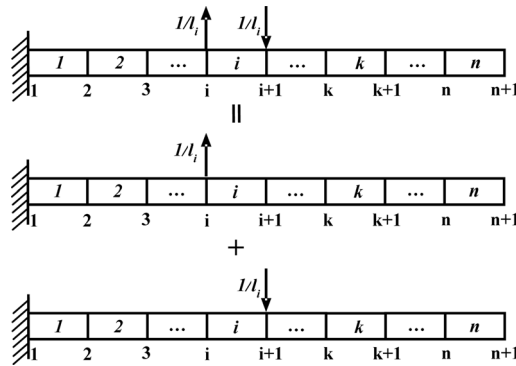


Fig. 3 Superimposition of loads

$$\theta_{k,i} = \frac{1}{l_k} \frac{[(\mathbf{F}_{k+1,i+1} - \mathbf{F}_{k+1,i}) - (\mathbf{F}_{k,i+1} - \mathbf{F}_{k,i})]}{l_i} \tag{3}$$

where $\mathbf{F}_{k,i}$ is the deflection at Node k resulting from a unit force at Node i , and it is actually one of the elements in the deflection flexibility matrix \mathbf{F} .

$\mathbf{F}_{k,i}$ can be assembled by translational modes as follows

$$\mathbf{F}_{k,i} = \sum_{r=1}^n \frac{\varphi_{kr}\varphi_{ir}}{\omega_r^2} \tag{4}$$

where φ_{ir} and φ_{kr} are the i th and k th components of the r th translational mode shape, respectively; ω_r is the r th circular modal frequency; n is the number of modes used here.

Likewise, we can obtain the ASHs of all other elements under this unit moment, and thus the i th column of the ASH flexibility matrix can be expressed as

$$\begin{bmatrix} \theta_{1,i} \\ \theta_{2,i} \\ \vdots \\ \theta_{i,i} \\ \theta_{i+1,i} \\ \vdots \\ \theta_{n-1,i} \\ \theta_{n,i} \end{bmatrix} = \begin{bmatrix} \frac{1}{l_1 l_i} (\mathbf{F}_{2,i+1} - \mathbf{F}_{2,i}) \\ \frac{1}{l_2 l_i} [(\mathbf{F}_{3,i+1} - \mathbf{F}_{3,i}) - (\mathbf{F}_{2,i+1} - \mathbf{F}_{2,i})] \\ \vdots \\ \frac{1}{l_i l_i} [(\mathbf{F}_{i+1,i+1} - \mathbf{F}_{i+1,i}) - (\mathbf{F}_{i,i+1} - \mathbf{F}_{i,i})] \\ \frac{1}{l_{i+1} l_i} [(\mathbf{F}_{i+2,i+1} - \mathbf{F}_{i+2,i}) - (\mathbf{F}_{i+1,i+1} - \mathbf{F}_{i+1,i})] \\ \vdots \\ \frac{1}{l_{n-1} l_i} [(\mathbf{F}_{n,i+1} - \mathbf{F}_{n,i}) - (\mathbf{F}_{n-1,i+1} - \mathbf{F}_{n-1,i})] \\ \frac{1}{l_n l_i} [(\mathbf{F}_{n+1,i+1} - \mathbf{F}_{n+1,i}) - (\mathbf{F}_{n,i+1} - \mathbf{F}_{n,i})] \end{bmatrix} \tag{5}$$

Substituting Eq. (4) into Eq. (5) yields the expressions of the i th column of the ASH flexibility in terms of translational modes

$$\begin{bmatrix} \theta_{1,i} \\ \theta_{2,i} \\ \vdots \\ \theta_{i,i} \\ \theta_{i+1,i} \\ \vdots \\ \theta_{n-1,i} \\ \theta_{n,i} \end{bmatrix} = \sum_{r=1}^n \frac{1}{\omega_r^2} \begin{bmatrix} \frac{1}{l_1 l_i} (\varphi_{2,r} \varphi_{i+1,r} - \varphi_{2,r} \varphi_{i,r}) \\ \frac{1}{l_2 l_i} [(\varphi_{3,r} \varphi_{i+1,r} - \varphi_{3,r} \varphi_{i,r}) - (\varphi_{2,r} \varphi_{i+1,r} - \varphi_{2,r} \varphi_{i,r})] \\ \vdots \\ \frac{1}{l_i l_i} [(\varphi_{i+1,r} \varphi_{i+1,r} - \varphi_{i+1,r} \varphi_{i,r}) - (\varphi_{i,r} \varphi_{i+1,r} - \varphi_{i,r} \varphi_{i,r})] \\ \frac{1}{l_{i+1} l_i} [(\varphi_{i+2,r} \varphi_{i+1,r} - \varphi_{i+2,r} \varphi_{i,r}) - (\varphi_{i+1,r} \varphi_{i+1,r} - \varphi_{i+1,r} \varphi_{i,r})] \\ \vdots \\ \frac{1}{l_{n-1} l_i} [(\varphi_{n,r} \varphi_{i+1,r} - \varphi_{n,r} \varphi_{i,r}) - (\varphi_{n-1,r} \varphi_{i+1,r} - \varphi_{n-1,r} \varphi_{i,r})] \\ \frac{1}{l_n l_i} [(\varphi_{n+1,r} \varphi_{i+1,r} - \varphi_{n+1,r} \varphi_{i,r}) - (\varphi_{n,r} \varphi_{i+1,r} - \varphi_{n,r} \varphi_{i,r})] \end{bmatrix} \\
 = \sum_{r=1}^n \frac{1}{\omega_r^2} \mathbf{R}_r \left[\frac{1}{l_i} (\varphi_{i+1,r} - \varphi_{i,r}) \right] \tag{6}$$

where \mathbf{R}_r is called the r th ASH mode shape here, and it is expressed in terms of the r th translational mode shape as follows

$$\mathbf{R}_r = \left[\frac{1}{l_1} \varphi_{2,r} \quad \frac{1}{l_2} (\varphi_{3,r} - \varphi_{2,r}) \quad \dots \quad \frac{1}{l_i} (\varphi_{i+1,r} - \varphi_{i,r}) \quad \frac{1}{l_{i+1}} (\varphi_{i+2,r} - \varphi_{i+1,r}) \quad \dots \quad \frac{1}{l_{n-1}} (\varphi_{n,r} - \varphi_{n-1,r}) \quad \frac{1}{l_n} (\varphi_{n+1,r} - \varphi_{n,r}) \right]^T \tag{7}$$

All columns of the ASH flexibility matrix can be obtained by applying a unit moment on each element sequentially. Stacking all columns, the ASH flexibility matrix \mathbf{F}_θ can be formed as follows

$$\mathbf{F}_\theta = \sum_{r=1}^n \frac{1}{\omega_r^2} \begin{bmatrix} \frac{1}{l_1} \varphi_{2,r} \\ \frac{1}{l_2} (\varphi_{3,r} - \varphi_{2,r}) \\ \vdots \\ \frac{1}{l_i} (\varphi_{i+1,r} - \varphi_{i,r}) \\ \frac{1}{l_{i+1}} (\varphi_{i+2,r} - \varphi_{i+1,r}) \\ \vdots \\ \frac{1}{l_{n-1}} (\varphi_{n,r} - \varphi_{n-1,r}) \\ \frac{1}{l_n} (\varphi_{n+1,r} - \varphi_{n,r}) \end{bmatrix} \left\| \begin{bmatrix} \frac{1}{l_1} \varphi_{2,r} \\ \frac{1}{l_2} (\varphi_{3,r} - \varphi_{2,r}) \\ \vdots \\ \frac{1}{l_i} (\varphi_{i+1,r} - \varphi_{i,r}) \\ \frac{1}{l_{i+1}} (\varphi_{i+2,r} - \varphi_{i+1,r}) \\ \vdots \\ \frac{1}{l_{n-1}} (\varphi_{n,r} - \varphi_{n-1,r}) \\ \frac{1}{l_n} (\varphi_{n+1,r} - \varphi_{n,r}) \end{bmatrix} \right. \tag{8}$$

$$= \sum_{r=1}^n \frac{1}{\omega_r^2} \mathbf{R}_r \mathbf{R}_r^T \quad (8)$$

where n is the number of modes needed to construct the ASH flexibility, which depends on the dynamic characteristics of structures. For structures with dense modes, more modes are needed than structures with sparse modes.

To make Eq. (8) applicable to any boundary conditions, the first component in the vector of \mathbf{R}_r , $\frac{1}{l_1} \varphi_{2,r}$, is adjusted to $\frac{1}{l_1} (\varphi_{2,r} - \varphi_{1,r})$, where $\varphi_{1,r}$ is the mode shape component associated with the support in the left.

Comparing Eq. (8) with Eq. (2), one can observe that the ASH flexibility matrix and the conventional deflection flexibility are assembled in the same way except that the former utilizes ASH mode shapes instead of translational modes. However, the components in the ASH flexibility matrix are associated with structural elements, while the components in the conventional deflection flexibility are associated with DOFs or nodes.

4. Damage detection using the ASH flexibility matrix

First, the change in the ASH flexibility matrices between the intact and damaged cases is calculated as

$$\Delta \mathbf{F}_\theta = \mathbf{F}_\theta^d - \mathbf{F}_\theta^u \quad (9)$$

Then the diagonals or the maximum absolute values of the components in each column in $\Delta \mathbf{F}_\theta$ are extracted, i.e.

$$\begin{aligned} \delta \mathbf{F}_\theta d &= [\delta \mathbf{F}_\theta d_1 \quad \delta \mathbf{F}_\theta d_2 \quad \dots \quad \delta \mathbf{F}_\theta d_i \quad \dots \quad \delta \mathbf{F}_\theta d_{n-1} \quad \delta \mathbf{F}_\theta d_n] \\ &= [\Delta \mathbf{F}_{\theta 11} \quad \Delta \mathbf{F}_{\theta 22} \quad \dots \quad \Delta \mathbf{F}_{\theta ii} \quad \Delta \mathbf{F}_{\theta, n-1, n-1} \quad \Delta \mathbf{F}_{\theta nn}] \end{aligned} \quad (10)$$

or

$$\begin{aligned} \delta \mathbf{F}_\theta m &= [\delta \mathbf{F}_\theta m_1 \quad \delta \mathbf{F}_\theta m_2 \quad \dots \quad \delta \mathbf{F}_\theta m_i \quad \dots \quad \delta \mathbf{F}_\theta m_{n-1} \quad \delta \mathbf{F}_\theta m_n] \\ &= [\max(\Delta \mathbf{F}_{\theta \cdot 1}) \quad \max(\Delta \mathbf{F}_{\theta \cdot 2}) \quad \dots \quad \max(\Delta \mathbf{F}_{\theta \cdot i}) \quad \dots \quad \max(\Delta \mathbf{F}_{\theta \cdot n-1}) \quad \max(\Delta \mathbf{F}_{\theta \cdot n})] \end{aligned} \quad (11)$$

where $\Delta \mathbf{F}_{\theta ii}$ and $\max(\Delta \mathbf{F}_{\theta \cdot i})$ are the i th diagonal and the component with the maximum absolute value in the i th column of $\Delta \mathbf{F}_\theta$, respectively. Each component in $\delta \mathbf{F}_\theta d$ or $\delta \mathbf{F}_\theta m$ represents the damage indicator of the corresponding element. If there is damage in a structure, the plot of extracted damage indicators exhibits a step-distribution, and the damage indicator associated with a damaged element exhibits a jump between two steps. By observing the “step and jump” in the magnitude distribution of damage indicators in the plot of $\delta \mathbf{F}_\theta d$ or $\delta \mathbf{F}_\theta m$ versus number of elements, damage can be directly localized to exact elements. Please note that the damage indicators are associated with structural elements instead of DOFs or nodes, because the components in the ASH flexibility matrix are associated with structural elements.

Using numerical derivation, Appendix 2 illustrates how the damaged element in the left side of

the beam (which is closer to the clamped end) affects the damage indicators (based on the ASH flexibility) of the following elements. It demonstrates that the proposed approach significantly reduces the contribution of the damaged element in the left to the damage indicators of the following elements to such extent that can be comparable with that from the following damaged elements. In this way, the damage indicator of an element mainly reflects the deflection change within the element itself. Therefore, the ASH flexibility circumvents the problem associated with the conventional deflection flexibility, and thus the damage indicators based on the ASH flexibility can identify multiple damage locations.

It is worth mentioning that, in some cases where it is difficult to obtain mass-normalized mode shapes, the normalization of restricting the length of the mode shapes to unity also works with the proposed method. However, the constructed flexibility will be pseudo-ASH flexibility.

5. Numerical examples

Using numerical examples, Example 1 illustrates the ability of the proposed approach for localizing multiple damage sites and quantifying the damage. Moreover, aiming at practical applications, the effects of both the number of the modes used and the number of measurement sensors on the damage detection results are investigated. In Example 2, the approach is applied to localize damage notches in a cantilever beam using simulated data.

5.1 Example 1

A cantilever beam is studied in this example. This beam is assumed to be made of aluminum with dimensions 2080 mm × 20 mm × 20 mm. Young’s modulus, mass density and Poisson ratio of the material are 70 Gpa, 2700 kg/m³ and 0.3, respectively. The Finite Element Analysis is used to calculate natural frequencies and mass-normalized mode shapes in this example. The beam is modeled using 26 beam elements, each of 80 mm long, with 52 DOFs, as shown in Fig. 1 (herein $n = 26$). The first 10 natural frequencies are listed in Table 1. Damage is simulated as a reduction in the stiffness of some elements in the model.

5.1.1 Damage localization and the effect of the number of modes used

In this case, the Young’s moduli in Elements 4 and 22 are reduced by 10% (Case 1). The first 10 natural frequencies for this case are also listed in Table 1. All 26 translational mode shapes normalized with respect to mass are used to assemble the ASH flexibility matrices for the intact and damaged structures. The damage indicators are extracted using Eqs. (10) and (11) and are plotted against element numbers in Fig. 4(a). In this figure, it is observed that the damage indicators are

Table 1 The first 10 natural frequencies for the intact and damaged cases (Hz)

Order	1	2	3	4	5	6	7	8	9	10
Intact	3.80	23.73	66.15	128.92	211.72	313.85	434.57	573.03	728.37	899.69
Case 1	3.78	23.73	66.31	129.36	213.12	318.16	444.72	591.85	758.34	944.36

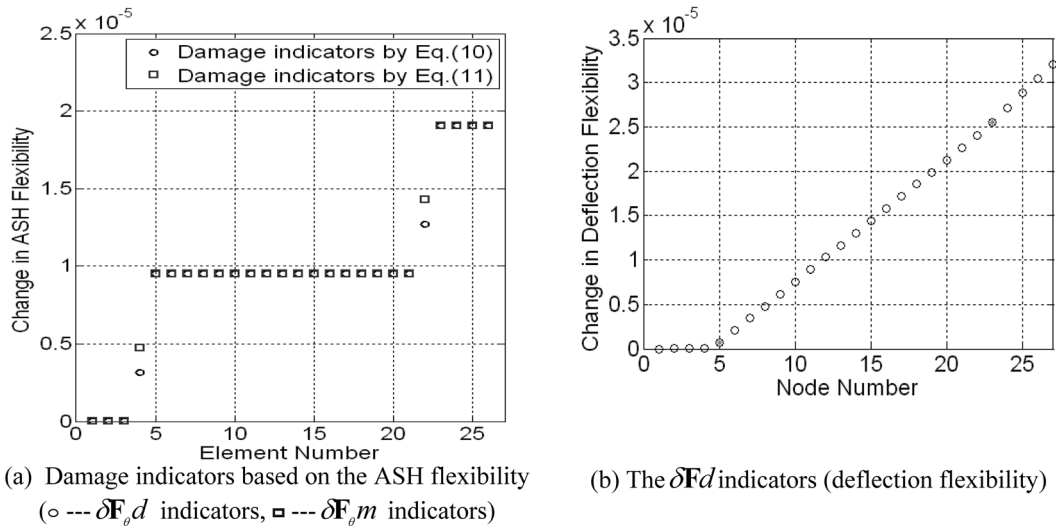


Fig. 4 Damage localization results using all 26 translational modes for Example 1

approximately distributed as two steps, and the heights of the two steps are identical. It suggests that two elements are damaged and their damage extents are equal. From the jump between each two steps, damage is localized to Elements 4 and 22. In particular, the $\delta F_{\theta d_4}$ is 1/3 times the height of the first step (the difference between $\delta F_{\theta d_5}$ and $\delta F_{\theta d_3}$) and the $\delta F_{\theta d_{22}}$ is 1/3 times the height of the second step (the difference between $\delta F_{\theta d_{23}}$ and $\delta F_{\theta d_{21}}$), while the $\delta F_{\theta m_4}$ and $\delta F_{\theta m_{22}}$ are 1/2 times the heights of the corresponding steps, which verify the analytical results given in Appendix 2. Also, we can tell that the relationship between the damage indicators of the damaged elements and the step heights is independent of the damage locations, which is one advantage of the proposed approach over the classical flexibility difference method. With this advantage, the proposed approach can quantify damage.

For comparison, the damage indicators extracted from the classical flexibility difference method are also presented, as shown in Fig. 4(b). In this figure, the δFd indicators are plotted against node numbers. It can be seen that the damage indicator at Node 5 starts to deviate from zero, suggesting that Element 4 is damaged. However, although Element 22 is also damaged, the change trend of the associated damage indicators (at Nodes 22 and 23) is almost the same as others nearby. Therefore, only one damaged element (Element 4) is identified using the traditional deflection flexibility, even though all 26 translational modes are used.

To examine the influence of the number of the modes used on the performance of the proposed approach, the damage indicators using different numbers of modes are extracted. Herein, only representative results corresponding to using the first two and five modes are presented, as shown in Figs. 5 and 6, respectively. From these results, one can conclude for this structure that: (1) if the first two modes are used, good damage localization results can be obtained by combining $\delta F_{\theta d}$ with $\delta F_{\theta m}$ indicators; (2) if the number of the modes used is greater than or equal to three, both the $\delta F_{\theta d}$ and $\delta F_{\theta m}$ indicators can identify the two damage sites (Elements 4 and 22). However, the damage locations have different influences on the magnitude distributions of the damage indicators extracted. Until the number of modes used increases to 5, the magnitude distribution of damage

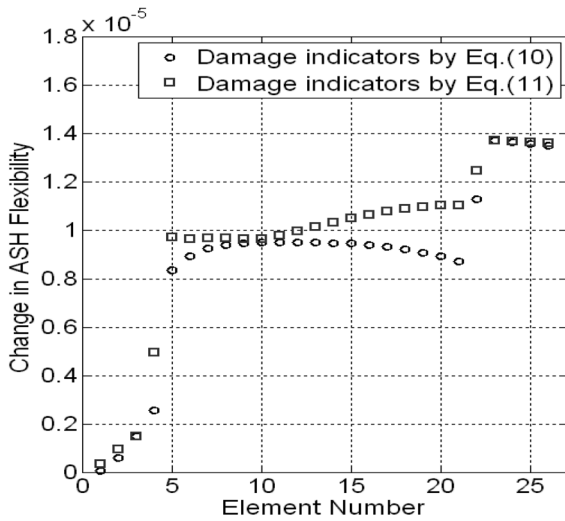


Fig. 5 Damage localization results using the first two modes for Example 1 (○ --- $\delta F_{\theta d}$ indicators; □ --- $\delta F_{\theta m}$ indicators)

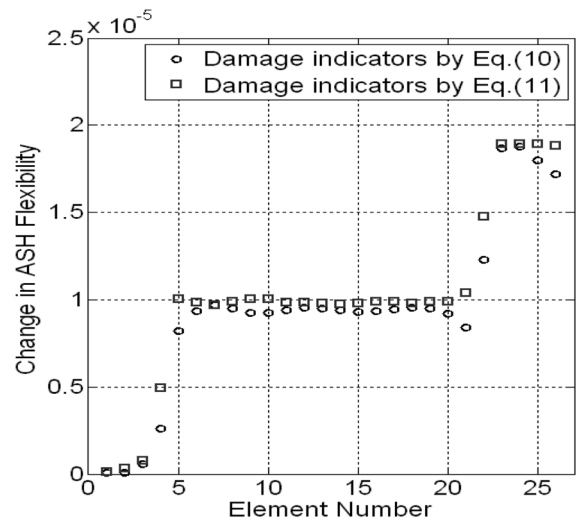


Fig. 6 Damage localization results using the first five modes for Example 1 (○ --- $\delta F_{\theta d}$ indicators; □ --- $\delta F_{\theta m}$ indicators)

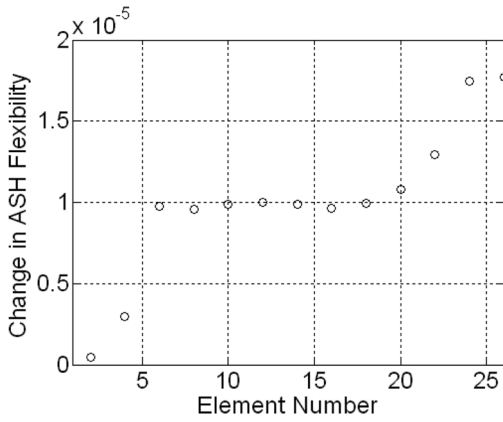
indicators are hardly affected by the damage locations. That is to say, to quantify the damage, the minimum of the modes used are five.

5.1.2 The effect of the number of measurement sensors

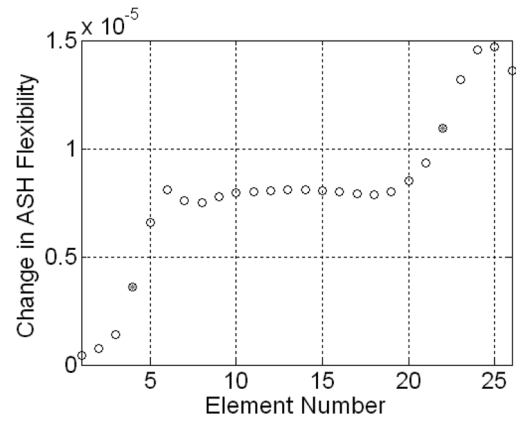
To investigate the robustness of the proposed approach in the face of sparse data, different numbers of mode shape components are used to simulate that the measurement DOFs are not complete. For the damaged case used in the previous section, it is assumed that thirteen, nine and five measurement sensors are deployed in the beam. Herein, only the first three modes are used to construct the ASH flexibility.

The $\delta F_{\theta m}$ indicators for these cases are presented in Fig. 7. From these figures, we can still see the step-type indicators and localize damage between two measurement sensors. In practical applications, we can uniformly deploy measurement sensors to roughly determine damaged regions, and then move sensors to the detected damaged regions to determine exactly damage locations, while one sensor should be remained at its original location for calibrating the data measured in different tests.

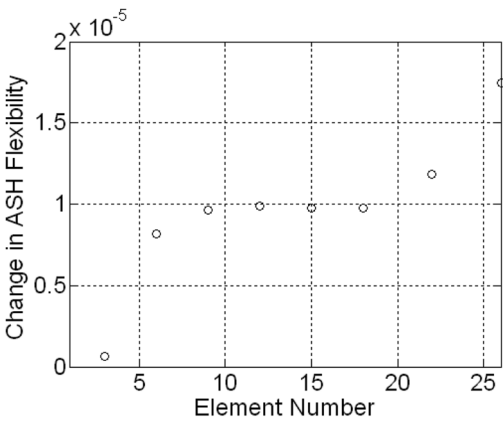
For a continuum structure, an attempt is made to exactly determine damaged elements by interpolating the incomplete mode shapes using a spline function. For the cases considered in this section, the interpolating operation is first performed on mode shapes and then a complete ASH flexibility is synthesized. The $\delta F_{\theta m}$ indicators extracted from the complete ASH flexibility matrices are presented in Fig. 8. It shows that the exact damaged elements can be identified when thirteen or nine DOFs in the vertical direction are measured. However, if only five DOFs in the vertical direction are measured, we still cannot determine exactly the damaged elements even though the interpolating operation is used. Therefore, a certain number of measurement points are required to exactly locate damage even when the interpolation among measured DOFs of mode shapes is used.



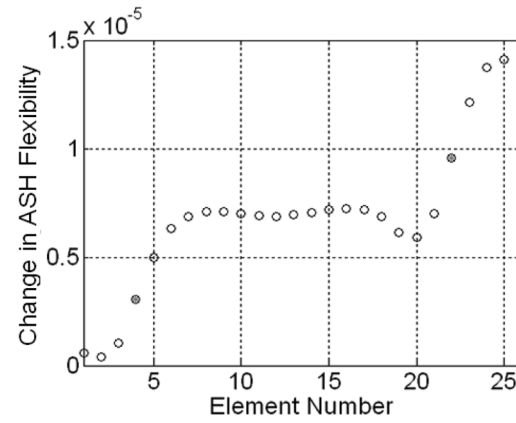
(a) Measurement at thirteen locations



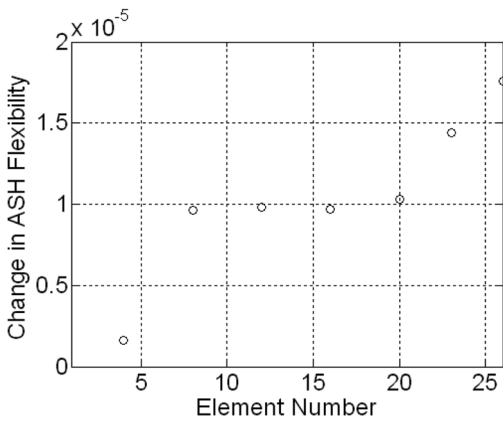
(a) Thirteen DOFs are measured



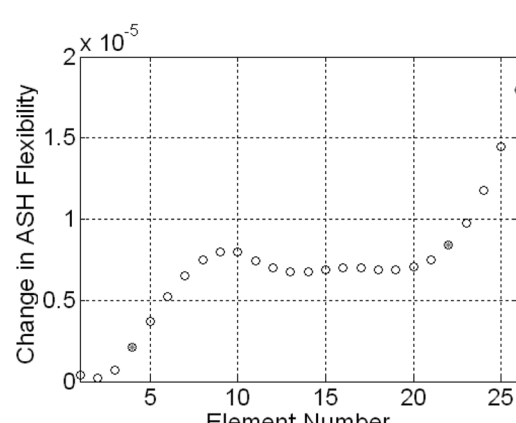
(b) Measurement at nine locations



(b) Nine DOFs are measured



(c) Measurement at five locations



(c) Five DOFs are measured

Fig. 7 Damage localization results with incomplete measurement of DOFs for Example 1

Fig. 8 Damage localization results when incomplete mode shapes are interpolated for Example 1

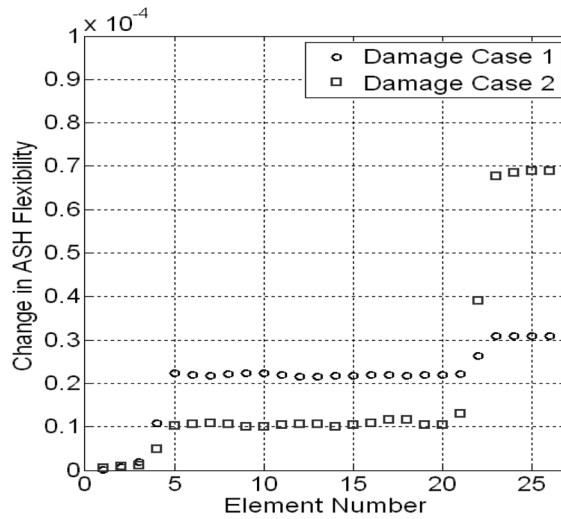


Fig. 9 Damage quantification results for Example 1 (Damage Case 1: Young’s moduli of elements 4 and 22 are reduced by 10% and 40%, respectively, Damage Case 2: Young’s moduli of elements 4 and 22 are reduced by 20% and 10%, respectively)

5.1.3 Damage quantification

To verify the capability of the proposed approach to determine relatively damage severity, various damage cases with different damage extents are considered, as shown in Fig. 9. As mentioned above (shown in Fig. 6), only if the number of the modes used is greater than or equal to 5, damage with equal extents in different elements produces identical step heights in the magnitude distribution of damage indicators, which does not depend on the damage locations. Therefore, the first five modes are used in these cases. For each case, the $\delta F_{\theta m}$ indicators are plotted in Fig. 9.

From the square markers shown in Fig. 9, one can infer that the damage extent in Element 22 is greater than that in Element 4 in Case 1 and the former is approximately four times the latter, which is consistent with the simulated damage scenario. Likewise, from the circle markers in Fig. 9, we can tell that the damage extent of Element 22 is approximately twice larger than that of Element 4 in this case.

5.2 Example 2: Notch localization

To further demonstrate the effectiveness of the proposed approach, a modal test of a cantilever beam is numerically simulated to obtain structural acceleration response and excitation time history. Modal parameters are identified from the acceleration response and excitation data. The material of the beam is assumed to be hot rolled, lightweight steel. Its cross-section is 80 mm high and 50 mm wide, and its web is 4.5 mm thick, as shown in Fig. 10(b). Its cross-sectional area and inertia moment are $9.58 \times 10^{-4} \text{ m}^2$ and $100.19 \times 10^{-8} \text{ m}^4$, respectively. The length of this beam is 1.98 m. The beam is modeled using 11 beam elements, each of 180 mm, with 12 nodes, as shown in Fig. 10(a). In this figure, normal and bold numbers indicate node numbers, and italic and bold numbers indicate element numbers.

Assume that viscous dissipation is included in the form of orthogonal damping with a magnitude

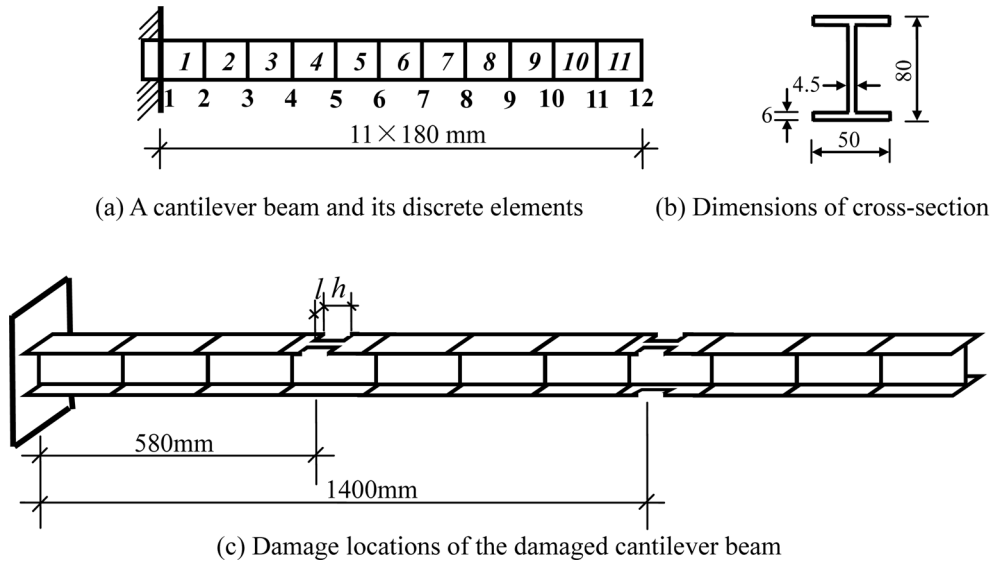


Fig. 10 A cantilever beam

Table 2 Damage cases of the cantilever beam in the simulation

Case	Damage locations	Slot depth h and slot length l
1	Upper flange, at $l = 580$ mm from the clamped end	$h = 20$ mm, $l = 20$ mm
	Upper and lower flange, at $l = 1400$ mm from the clamped end	$h = 20$ mm, $l = 20$ mm
2	Upper flange, at $l = 580$ mm from the clamped end	$h = 15$ mm, $l = 20$ mm
	Upper and lower flange, at $l = 1400$ mm from the clamped end	$h = 15$ mm, $l = 20$ mm
3	Upper flange, at $l = 580$ mm from the clamped end	$h = 10$ mm, $l = 20$ mm
	Upper and lower flange, at $l = 1400$ mm from the clamped end	$h = 10$ mm, $l = 20$ mm

of 1% of critical in each mode of the structure. Band-limited random white noise process is applied in the vertical direction at all nodes to simulate ambient excitation. Simulated acceleration responses in the vertical direction are computed using Newmark-Beta integration. It is assumed that the acceleration and excitation time history are recorded at the sampling rate of 4096 Hz. To simulate practical field conditions, Gaussian white noise with the mean value of zero and an RMS (root-mean-square) equal to 5% of the RMS of the corresponding response is added to the acceleration responses.

Damage is simulated by introducing a pair of symmetric notches in upper and lower flanges, as shown in Fig. 10(c). Damage cases considered in this study are specified in Table 2.

The procedures for detecting damage using the proposed approach are as follows. First, Eigensystem Realization Algorithm (ERA) is applied to identify natural frequencies and translational mode shapes, and then the identified mode shapes are normalized with respect to mass. Second, the ASH mode shapes are computed using Eq. (7), and then the ASH flexibility matrices for the intact and damaged beams are assembled using Eq. (8). In this example, the first five

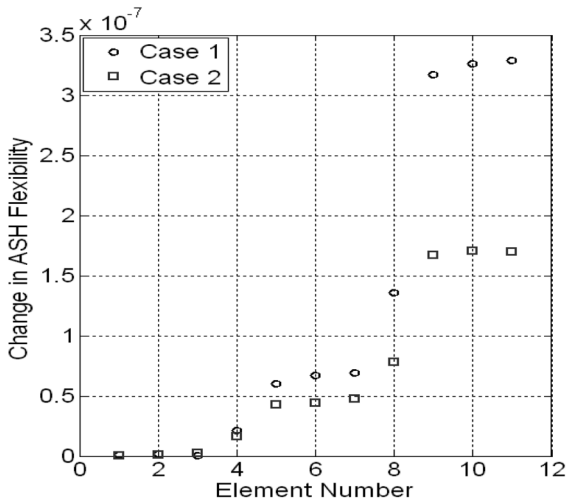


Fig. 11 Damage detection results of Case 1 and Case 2 in Example 2 (Case 1 and Case 2 are listed in Table 2)

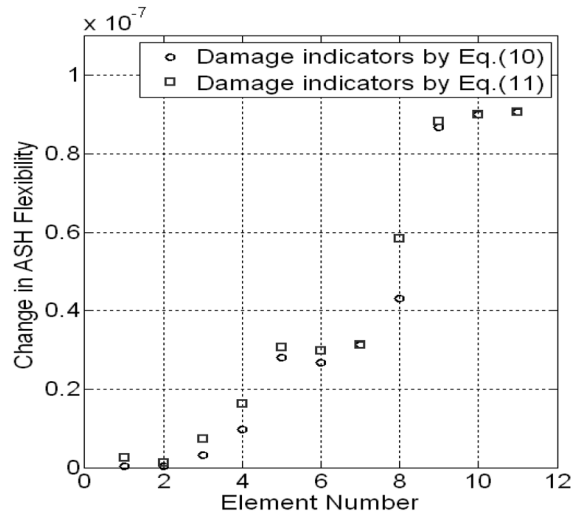


Fig. 12 Damage detection results of Case 3 in Example 2 (Case 3 is listed in Table 2; ○ --- $\delta F_{\theta d}$ indicators; □ --- $\delta F_{\theta m}$ indicators)

identified modes are used. Finally, damage indicators are extracted using Eq. (10) or Eq. (11).

Both the $\delta F_{\theta d}$ and $\delta F_{\theta m}$ indicators are extracted for each case. For Cases 1 and 2, both damage indicators deliver similar information on damage, and thus only $\delta F_{\theta d}$ indicators are presented, as shown in Fig. 11. It suggests that damage occurs in Elements 4 and 8, and the damage extent of Element 8 is approximately twice that of Element 4, which is consistent with the damage scenarios specified in Table 2. For damage with a smaller extent, like Case 3, damage can be easily localized by observing both the $\delta F_{\theta d}$ and $\delta F_{\theta m}$ indicators, as shown in Fig. 12.

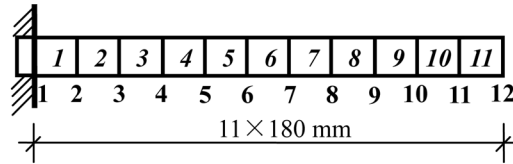
6. Experimental application

To further validate the performance of the proposed approach, experimental tests are conducted on a cantilever beam and a simply supported beam.

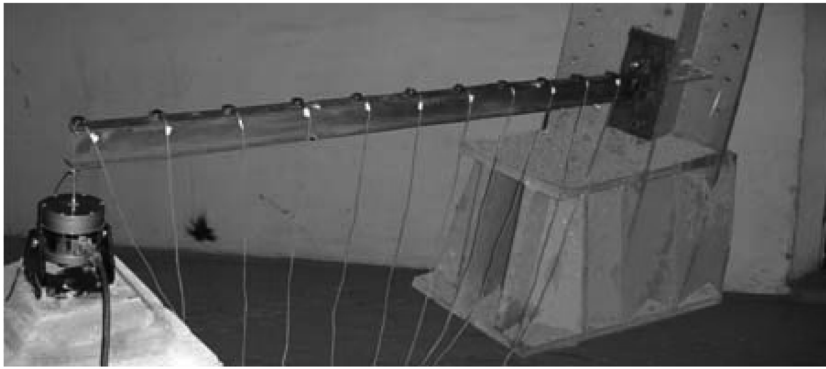
6.1 Description of experiment

Both beams are flanged beams made of hot rolled, lightweight Q235 steel. The cross-section and material properties of both the cantilever beam and simply supported beams are the same as that in the numerical example in Section 5.2. The lengths of the cantilever beam and the simply supported beam are 1.98 and 1.8 m, respectively. The finite element models of both beams are shown in Fig. 13(a) and Fig. 14(a), respectively.

The LMS SCADAS III system is used to acquire the dynamic data. PCB capacitive accelerometers are employed to measure acceleration responses, and 11 accelerometers are deployed at Nodes 2-12 of both beams, as shown in Figs. 13 and 14. The beams are subjected to band-limited white noise (0-2000 Hz), and the excitation setup consists of a JZK-5 kg shaker, a charge amplifier

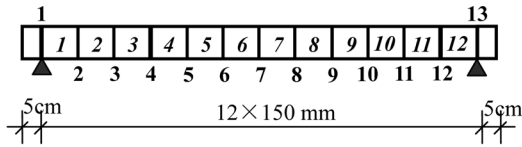


(a) The FEM of the cantilever beam

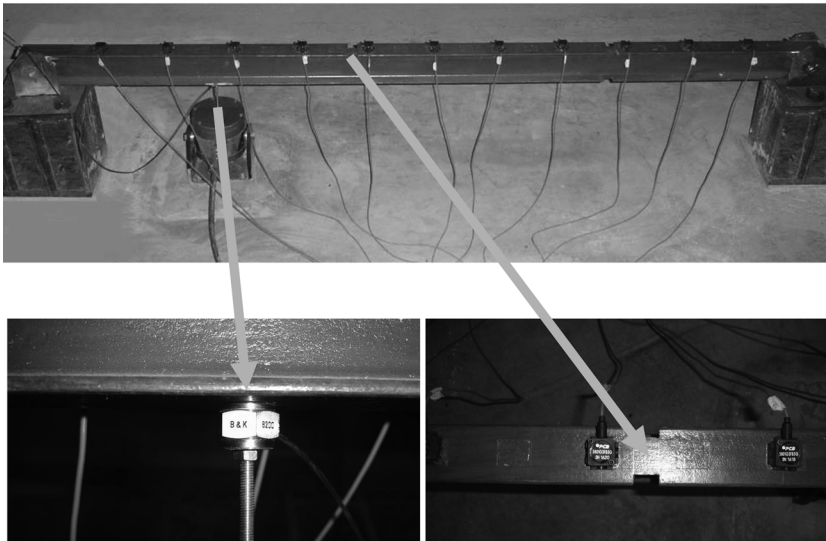


(b) Damage locations and sensor placement for damaged cantilever beam

Fig. 13 The cantilever beam and the experimental setup



(a) The FEM of the simply supported beam



(b) Damage locations and sensor placement for simply supported beam

Fig. 14 The simply supported beam and the experimental setup

Table 3 Damage cases of the simply supported beam in the experiment

Case	Damage locations	Slot depth h and slot length l
1	Upper flange, at $l = 705$ mm from the simply supported end	$h = 20$ mm, $l = 20$ mm
	Upper and lower flange, at $l = 1305$ mm from the simply supported end	$h = 20$ mm, $l = 20$ mm
2	Upper flange, at $l = 705$ mm from the simply supported end	$h = 15$ mm, $l = 20$ mm
	Upper and lower flange, at $l = 1305$ mm from the simply supported end	$h = 15$ mm, $l = 20$ mm
3	Upper flange, at $l = 705$ mm from the simply supported end	$h = 10$ mm, $l = 20$ mm
	Upper and lower flange, at $l = 1305$ mm from the simply supported end	$h = 10$ mm, $l = 20$ mm

and a power amplifier. The cantilever beam is excited at the free end, and the simply supported beam is excited at the location which is 40 cm away from the simply supported end. A force transducer of B&K 8200 is employed to acquire the excitation data. The sampling frequency of acceleration responses and excitation data is 6400 Hz and the sampling duration is 50 seconds.

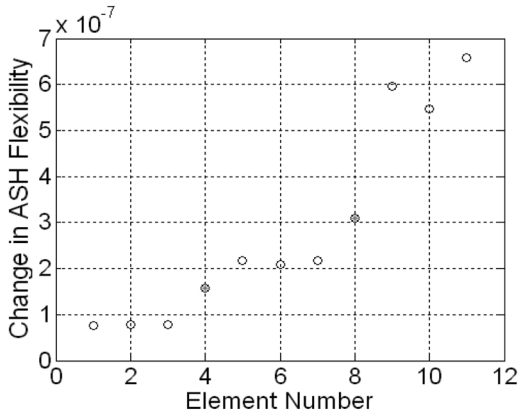
Damage is simulated by introducing a pair of symmetric notches in upper and lower flanges. Damage cases in the cantilever beam are the same as Example 2 in Section 5.2, as shown in Table 2. Damage cases of the simply supported beam are specified in Table 3. Modal experiments are performed on the intact and damaged beams, sequentially.

6.2 Experimental results

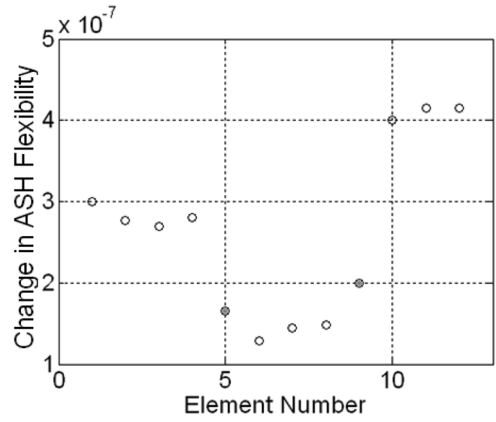
Both damage indicators based on the ASH flexibility, $\delta F_{\theta d}$ and $\delta F_{\theta m}$, are extracted using the procedures summarized in Section 5.2. Because similar results are obtained from the two indicators, only and the $\delta F_{\theta m}$ indicators are presented in the sequel.

For the cantilever beam, the first six, five, four and three modes are used to extract the damage indicators, respectively. Similar results are obtained. Only the $\delta F_{\theta m}$ indicators corresponding to using the first six modes are presented, as shown in Fig. 15. From Fig. 15(a), it is observed that: (1) there are two steps in the magnitude distribution of damage indicators. It suggests that two damage sites occur in the beam, namely Elements 4 and 8; (2) the height of the second step is evidently greater than that of the first one, and the former is approximately twice the latter. It suggests that the damage extent of the damage in Element 8 is twice that of the damage in Element 4. All the observations are consistent with the damage scenario specified in Case 1. Figs. 15(b) and (c) present the $\delta F_{\theta m}$ indicators for Damage Cases 2 and 3 of the cantilever beam, respectively. It can be seen that the two notches with the depths of 15 mm and 10 mm are successfully localized by the proposed approach.

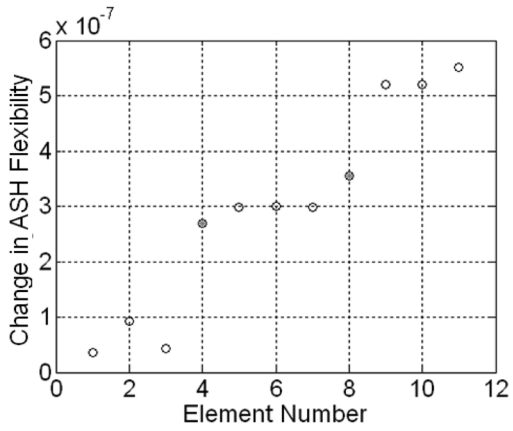
For the three damaged cases of the simply supported beam, the $\delta F_{\theta m}$ indicators corresponding to using the first four modes are plotted in Fig. 16. It can be found that: (1) there exist two steps in the magnitude distribution of damage indicators. It suggests that two elements (Elements 5 and 9) in the simply supported beam are damaged; (2) the height of the second step is appreciably greater than the first one and the former is approximately twice the latter. It suggests the damage extent of Element 9 is twice that of Element 5.



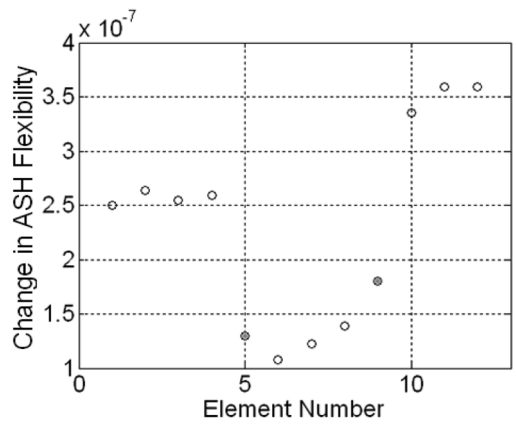
(a) Damage case 1



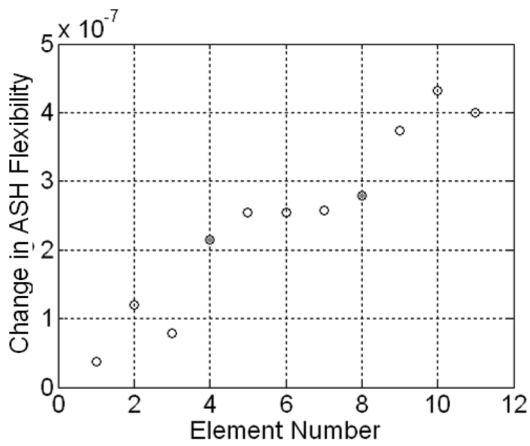
(a) Damage case 1



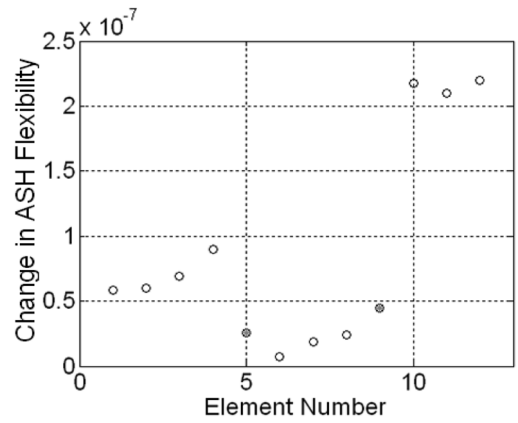
(b) Damage Case 2



(b) Damage case 2



(c) Damage case 3



(c) Damage case 3

Fig. 15 Damage detection results for the experimental cantilever beam

Fig. 16 Damage detection results for the experimental simply supported beam

Table 4 The first six modal parameters for the intact and three damaged cases of the cantilever beam

Order	Case	Intact		Case 1		Case 2		Case 3	
		Freq. (Hz)	Damping ratio (%)						
1		21.33	1.02	21.29	1.14	21.13	1.18	21.36	1.15
2		131.82	0.12	129.39	0.24	130.41	0.20	131.06	0.13
3		356.60	0.17	343.50	0.21	350.05	0.19	353.45	0.21
4		664.73	0.42	655.93	0.87	659.92	0.44	663.60	0.52
5		1153.00	0.44	1033.10	0.40	1038.80	0.50	1103.40	0.26
6		1521.00	0.29	1452.50	0.80	1476.90	0.46	1498.10	0.36

Table 5 The first four modal parameters for the intact and three damaged cases of the simply supported beam

Order	Case	Intact		Case 1		Case 2		Case 3	
		Freq. (Hz)	Damping ratio (%)						
1		79.77	0.98	77.35	0.71	78.77	0.80	79.38	0.87
2		279.62	0.80	271.13	1.04	275.45	0.73	277.84	0.79
3		542.67	1.18	539.94	0.73	540.81	1.11	542.48	1.31
4		796.30	0.76	780.79	0.86	783.84	0.83	791.87	0.86

7. Conclusions

The incapability of the classical flexibility difference method for localizing multiple damage sites is analyzed. A more feasible flexibility for localizing damage in beam-type structures, the Angle-between-String-and-Horizon (ASH) flexibility, is proposed, and a damage detection method based on the ASH flexibility is developed. This proposed approach has the following advantages. First, multiple damage locations can be directly indicated by a step distribution of damage indicators and it holds true for structures with arbitrary boundary conditions. Second, the height of each step is related to damage extent and does not depend on the damage location if enough number of modes are available. Therefore, this approach can determine relatively damage severity from the heights of steps. On the contrary, the damage indicators based on the conventional deflection flexibility are affected by damage locations and thus they can't quantify damage. Finally, each damage indicator is associated with a structural member or element instead of a node or DOF, and thus this method can be applied to relatively complex structures.

The numerical and experimental results suggest that the proposed approach has the ability to localize multiple damage sites in beam-type structures in the presence of measurement noises. It only requires a few low-frequency modes. When the measured DOFs are not complete, the method can still localize damage between two measurement sensors.

However, the capability of the proposed approach hinges on the quality of the estimated ASH flexibility. The estimation accuracy of the ASH flexibility depends, in turn, on the quality of the measured data and the identified modal parameters. In addition, although the method has been

successfully applied to beam-type structures, further work should be done to generalize this method to other types of structures. Actually, this approach has already been extended to truss structures to perform damage localization at the member level (Yan *et al.* 2009).

Acknowledgements

The authors would like to acknowledge the National Natural Science Foundation of China for financial support under Grant Nos. 50579008 and 50708029.

References

- Harri, K., Guillaume, P. and Vanlanduit, S. (2008), "On-line damage detection on a wing panel using transmission of multisine ultrasonic waves", *NDT & E Int.*, **41**(4), 312-317.
- Unger, J.F., Teughels, A. and De Roeck, G. (2006), "System identification and damage detection of a prestressed concrete beam", *J. Struct. Eng.*, **132**(11), 1691-1698.
- Doebbling, S.W., Farrar, C.R. and Prime, M.B. (1996), "A summary review of vibration-based damage identification methods", Report of Los Alamos National Laboratory.
- Yang, J.N., Lin, S., Huang, H. and Zhou, L. (2006), "An adaptive extended kalman filter for structural damage identification", *Struct. Control Health Monit.*, **13**(4), 849-867.
- Yang, J.N., Pan, S. and Lin, S. (2007), "Least-squares estimation with unknown excitations for damage identification of structures", *J. Eng. Mech.*, **133**(1), 12-21.
- Sakellariou, J.S. and Fassois, S.D. (2006), "Stochastic output error vibration-based damage detection and assessment in structures under earthquake excitation", *J. Sound Vib.*, **297**(3-5), 1048-1067.
- Huang, Y., Meyer, D. and Nemat-Nasser, S. (2009), "Damage detection with spatially distributed 2D Continuous Wavelet Transform", *Mech. Mater.*, **41**, 1096-1107.
- Pakrashi, V., Basu, B. and O'Connor, A. (2007), "Structural damage detection and calibration using a wavelet-kurtosis technique", *Eng. Struct.*, **29**, 2097-2108.
- Law, S.S., Li, X.Y., Zhu, X.Q. and Chan, S.L. (2005), "Structural damage detection from wavelet packet sensitivity", *Eng. Struct.*, **27**, 1339-1348.
- Basu, B. (2005), "Identification of stiffness degradation in structures using wavelet analysis", *Constr. Build. Mater.*, **19**(9), 713-721.
- Yan, G., Duan, Z. and Ou, J. (2009), "Structural damage detection using residual forces based on wavelet transform", *Mech. Syst. Signal Pr.*, **24**, 224-239.
- Lee, J.J., Lee, J.W., Yi, J.H., Yun, C.B. and Jung, H.Y. (2005), "Neural networks-based damage detection for bridges considering errors in baseline finite element models", *J. Sound Vib.*, **280**(3-5), 555-578.
- da Silva, S., Dias Jr., M., Lopes Jr., V. and Brennan, M.J. (2008), "Structural damage detection by fuzzy clustering", *Mech. Syst. Signal Pr.*, **22**, 1636-1649.
- Lua, Z.R. and Law, S.S. (2007), "Features of dynamic response sensitivity and its application in damage detection", *J. Sound Vib.*, **303**, 305-329.
- D' Souza, K. and Epureanu, B.I. (2008), "Multiple augmentations of nonlinear systems and generalized minimum rank perturbations for damage detection", *J. Sound Vib.*, **316**, 101-121.
- Galvanetto, U. and Violaris, G. (2007), "Numerical investigation of a new damage detection method based on proper orthogonal decomposition", *Mech. Syst. Signal Pr.*, **21**, 1346-1361.
- Guo, H.Y. (2006), "Structural damage detection using information fusion technique", *Mech. Syst. Signal Pr.*, **20**, 1173-1188.
- Li, H., Deng, X. and Dai, H. (2007), "Structural damage detection using the combination method of EMD and wavelet analysis", *Mech. Syst. Signal Pr.*, **21**, 298-306.
- Poudel, U.P., Fu, G. and Ye, J. (2005), "Structural damage detection using digital video imaging technique and

- wavelet transformation”, *J. Sound Vib.*, **286**(4-5), 869-895.
- Siringoringo, D.M. and Fujino, Y. (2006), “Experimental study of laser Doppler vibrometer and ambient vibration for vibration-based damage detection”, *Eng. Struct.*, **28**, 1803-1815.
- Yan, G., Guo, W., Dyke, S. and Lu, C. (2010), “Experimental Validation of a Multi-Level Damage Localization Technique with Distributed Computation”, Special Issue of *Smart Structures and Systems* on Wireless Sensors for Civil Infrastructure Monitoring, March.
- Doebbling, S.W. and Peterson, L.D. (1997), “Computing statically complete flexibility from dynamically measured flexibility”, *J. Sound Vib.*, **205**, 631-645.
- Doebbling, S.W. and Farrar, C.R. (1996), “Computation of Structural Flexibility for Bridge Health Monitoring Using Ambient Modal Data”, *Proceedings of 11th ASCE Engineering Mechanics Conference*, 1114-1117.
- Pandey, A.K. and Biswas, M. (1994), “Damage detection in structures using changes in flexibility”, *J. Sound Vib.*, **169**, 3-17.
- Pandey, A.K. and Biswas, M. (1995), “Experimental verification of flexibility difference method for locating damage in structures”, *J. Sound Vib.*, **184**, 311-328.
- Doebbling, S.W., Peterson, L.D. and Alvin, K.F. (1998), “Experimental Determination of Local Structural Stiffness by Disassembly of Measured Flexibility Matrices”, *J. Vib. Acoust.*, **120**, 949-957.
- Park, K.C., Reich, G.W. and Alvin, K.F. (1997), “Damage detection using localized flexibilities”, *Structural Health Monitoring, Current Status and Perspectives*, Ed. F.K. Chang, Technomic Publishers.
- Aoki, Y. and Byon, O.I. (2001), “Damage detection of CFRP pipes and shells by using localized flexibility method”, *Adv. Composite Mater.*, **10**, 189-198.
- Robinson, N.A., Peterson, L.D. and James, G.H. (1996), “Health monitoring of aircraft structures using experimental flexibility matrices”, *AIAA Meeting Paper 96-1304*, 328-337.
- Bernal, D. and Gunes, B. (2004), “Flexibility based approach for damage characterization: benchmark application”, *J. Eng. Mech.*, **130**, 61-70.
- Gao, Y. and Spencer, B.F. (2002), “Flexibility-based damage location employing ambient vibration”, *Proceedings of the 15th ASCE Engineering Mechanics Conference*, New York.
- Yan, G., Duan, Z., Ou, J. and Spencer, B.F. (2005), “Damage localization in ambient vibration by constructing proportional flexibility matrix”, *J. Sound Vib.*, **284**, 455-466.
- Yan, G., Guo, W., Dyke, S., Hackmann, G. and Lu, C. (2010), “Experimental validation of a multi-level damage localization technique with distributed computation”, *Smart Struct. Syst.*, **6**(5), 561-578.

Appendix 1: The influence of damage in Element 4 on damage indicators based on deflection flexibility

In order to further demonstrate how the damage in Element 4 affects the damage indicators based on deflection flexibility, a simple cantilever beam with 7 elements and 14 DOFs is considered, as shown in Fig. A1(1). Assume that the bending stiffness of each element of the intact beam is EI , while the Young's moduli in Elements 4 and 22 of the damaged beam are reduced to αE ($0 < \alpha \leq 1$). Herein the diagonals in $\Delta \mathbf{F}$ are selected as the measurement of the change in flexibility. Based on the physical significance of flexibility \mathbf{F} , the diagonals in \mathbf{F} represent the displacement at each node resulting from a unit force applied at that node. \mathbf{F}_{ii}^u and \mathbf{F}_{ii}^d are first obtained by the Graphic Multiplication Method and then the change in the diagonals of \mathbf{F} from the damaged state to the intact state is computed as follows

$$\delta \mathbf{F}d(i) = \mathbf{F}_{ii}^d - \mathbf{F}_{ii}^u$$

where the superscripts u and d denote the undamaged and damaged structures. In particular,

$$\begin{aligned} \delta \mathbf{F}d_1 &= 0 \\ \delta \mathbf{F}d_2 &= \mathbf{F}_{22}^d - \mathbf{F}_{22}^u = \frac{L^3}{3EI} - \frac{L^3}{3EI} = 0 \\ \delta \mathbf{F}d_3 &= \mathbf{F}_{33}^d - \mathbf{F}_{33}^u = \frac{8L^3}{3EI} - \frac{8L^3}{3EI} = 0 \\ \delta \mathbf{F}d_4 &= \mathbf{F}_{44}^d - \mathbf{F}_{44}^u = \frac{9L^3}{EI} - \frac{9L^3}{EI} = 0 \\ \delta \mathbf{F}d_5 &= \mathbf{F}_{55}^d - \mathbf{F}_{55}^u = \frac{L^3}{3E_d I} - \frac{L^3}{3EI} = \frac{L^3}{3EI} \left(\frac{1-\alpha}{\alpha} \right) \\ \delta \mathbf{F}d_6 &= \mathbf{F}_{66}^d - \mathbf{F}_{66}^u = \frac{11L^3}{6E_d I} - \frac{11L^3}{6EI} = \frac{11L^3}{6EI} \left(\frac{1-\alpha}{\alpha} \right) \\ \delta \mathbf{F}d_7 &= \mathbf{F}_{77}^d - \mathbf{F}_{77}^u = \frac{38L^3}{6E_d I} - \frac{38L^3}{6EI} = \frac{38L^3}{6EI} \left(\frac{1-\alpha}{\alpha} \right) \\ \delta \mathbf{F}d_8 &= \mathbf{F}_{88}^d - \mathbf{F}_{88}^u = \left(\frac{74L^3}{6E_d I} - \frac{74L^3}{6EI} \right) + \left(\frac{L^3}{3E_d I} - \frac{L^3}{3EI} \right) = \frac{76L^3}{6EI} \left(\frac{1-\alpha}{\alpha} \right) \end{aligned}$$

The above equations and Fig. A1 suggest that the values of $\delta \mathbf{F}d_i$ ($i=5, 6, 7, 8$) is only related to the area(s) (in the Graphic Multiplication Method) associated with the damaged element(s). For instance, the value of $\delta \mathbf{F}d_5$ is related to the area of the triangle to the right of Fig. A1(5), and the values of $\delta \mathbf{F}d_6$ and $\delta \mathbf{F}d_7$ are related to the area of the trapezium to the right of Fig. A1(6) and Fig. A1(7), respectively. The value of $\delta \mathbf{F}d_8$ is related to the areas of both the trapezium and the triangle to the right of Fig. A1(8).

The analytical results suggest that: 1) the damage in Element 4 doesn't affect the damage indicators at Nodes from 1 to 4; 2) the damage in Element 4 makes $\delta \mathbf{F}d_5$ start to deviate from zero, and it also makes $\delta \mathbf{F}d_i$ ($i=6, 7$) non-zero although Elements 5 and 6 are not damaged. Also, the farther the i th node is from the clamped end, the greater the damage indicator $\delta \mathbf{F}d_i$ ($i=6, 7$) will be. To be exact, $\delta \mathbf{F}d_6$ is 5.5 times $\delta \mathbf{F}d_5$, and $\delta \mathbf{F}d_7$ is 19 times $\delta \mathbf{F}d_5$. It is important to note that $\delta \mathbf{F}d_8$ includes not only the contribution from the damage in Element 4 but also that from Element 7. Because the former is 37 times greater than the latter, the increase in deflection at Node 8 induced by the damage in Element 7 is masked by the increase in deflection at Node 8 induced by the damage in Element 4. This is the very reason why the damage in Element 7 cannot be identified.

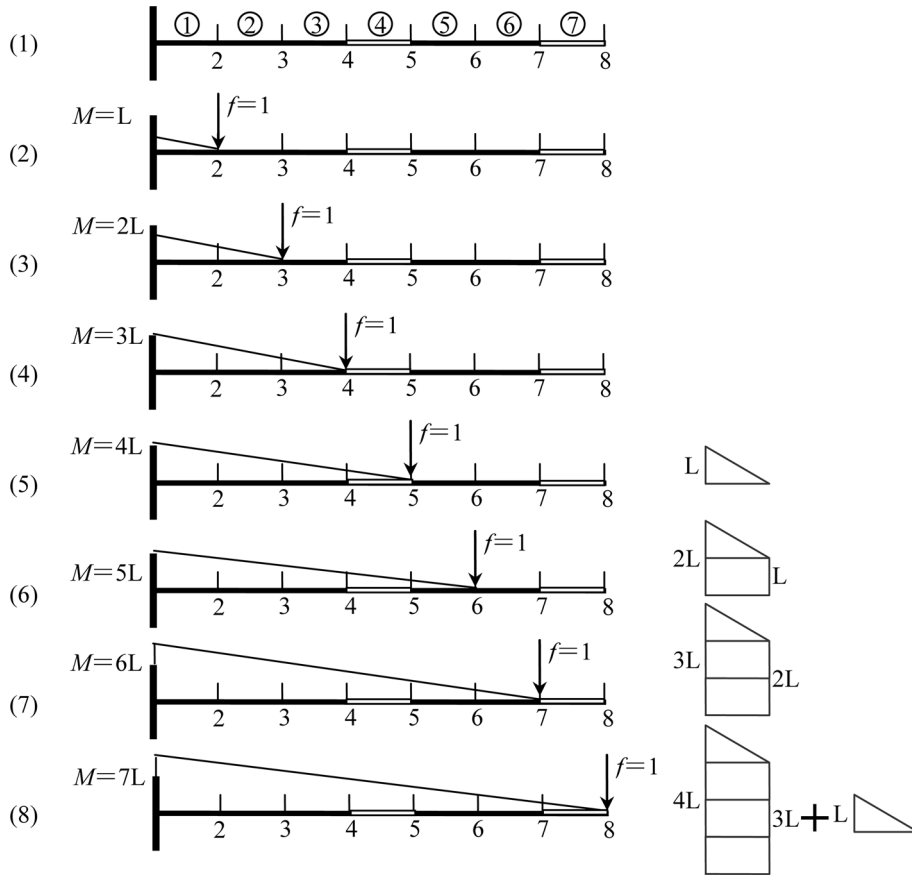


Fig. A1 Influence of damage in Element 4 on δFd indicators

Appendix 2: The influence of damage in Element 4 on damage indicators based on the ASH flexibility

The same example as in Appendix 1 is considered. Herein the diagonals in the difference between the ASH flexibility matrices before and after damage are selected as the measurement of the change in the ASH flexibility. The diagonals in an ASH flexibility represent the ASHs of each element resulting from a unit moment in the form of a pair of parallel forces with equal amplitudes but opposite directions applied at two nodes of this element. $F_{\theta ii}^u$ and $F_{\theta ii}^d$ are first computed by the Graphic Multiplication Method and then the difference in the diagonals in ASH flexibility from the damaged state to the intact state is obtained as follows

$$\delta F_{\theta} d_i = F_{\theta ii}^d - F_{\theta ii}^u$$

where the superscripts u and d denote the undamaged and damaged structures. In particular

$$\delta F_{\theta} d_1 = F_{\theta 11}^d - F_{\theta 11}^u = \frac{L}{3EI} - \frac{L}{3EI} = 0$$

$$\delta F_{\theta} d_2 = F_{\theta 22}^d - F_{\theta 22}^u = \frac{4L}{3EI} - \frac{4L}{3EI} = 0$$

$$\delta \mathbf{F}_\theta d_3 = \mathbf{F}_{\theta 33}^d - \mathbf{F}_{\theta 33}^u = \frac{7L}{3EI} - \frac{7L}{3EI} = 0$$

$$\delta \mathbf{F}_\theta d_4 = \mathbf{F}_{\theta 44}^d - \mathbf{F}_{\theta 44}^u = \frac{L}{3E_d I} - \frac{L}{3EI} = \frac{L}{3EI} \left(\frac{1-\alpha}{\alpha} \right)$$

$$\delta \mathbf{F}_\theta d_5 = \mathbf{F}_{\theta 55}^d - \mathbf{F}_{\theta 55}^u = \frac{L}{E_d I} - \frac{L}{EI} = \frac{L}{EI} \left(\frac{1-\alpha}{\alpha} \right)$$

$$\delta \mathbf{F}_\theta d_6 = \mathbf{F}_{\theta 66}^d - \mathbf{F}_{\theta 66}^u = \frac{L}{E_d I} - \frac{L}{EI} = \frac{L}{EI} \left(\frac{1-\alpha}{\alpha} \right)$$

$$\delta \mathbf{F}_\theta d_7 = \mathbf{F}_{\theta 77}^d - \mathbf{F}_{\theta 77}^u = \left(\frac{L}{E_d I} - \frac{L}{EI} \right) + \left(\frac{L}{3E_d I} - \frac{L}{3EI} \right) = \frac{4L}{3EI} \left(\frac{1-\alpha}{\alpha} \right)$$

Similar to Appendix 1, the value of $\delta \mathbf{F}_\theta d_4$ is related to the area of the triangle to the right of Fig. 2(4), and the values of $\delta \mathbf{F}_\theta d_5$ and $\delta \mathbf{F}_\theta d_6$ are related to the area of the rectangle to the right of Fig. 2(5) and Fig. 2(6), respectively. And the value of $\delta \mathbf{F}_\theta d_8$ is related to the areas of both the rectangle and the triangle to the right of Fig. 2(7).

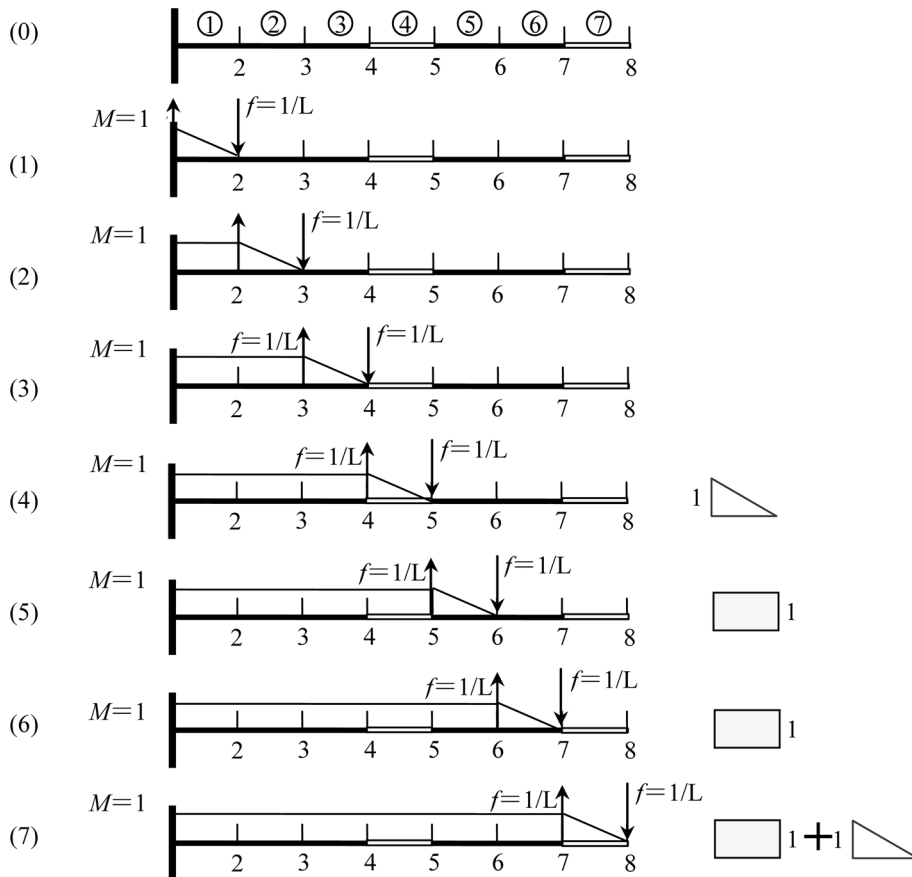


Fig. A2 Influence of damage in Element 4 on $\delta \mathbf{F}_\theta d$ indicators

As can be seen from the above equations, $\delta\mathbf{F}_\theta d_1$, $\delta\mathbf{F}_\theta d_2$ and $\delta\mathbf{F}_\theta d_3$ are zero because the first damaged element (Element 4) is not located between the clamped end and Node 4. The damage indicator of Element 4 starts to deviate from zero and the damage indicators of Elements from 5 to 7 are not zero due to the existence of the damage in Element 4. Unlike the conventional flexibility-based damage indicators, the influence of the damage in Element 4 on damage indicators of Elements from 5 to 7 does not increase with the distance of the elements away from the clamped end. To be exact, the damage indicators of the damaged elements ($\delta\mathbf{F}_\theta d_4$) are located at 1/3 times the height of the corresponding steps (equal to $\delta\mathbf{F}_\theta d_5 - \delta\mathbf{F}_\theta d_3$). By analogy, if the $\delta\mathbf{F}_{\theta m}$ indicators are used, the damaged indicators of the damaged elements are located 1/2 times the height of the corresponding steps. It can be seen that the application of the ASH flexibility doesn't completely eliminate the contribution of the damaged element in the left side to the damage indicators associated with the following elements. However, by using the ASH flexibility, the contribution of the damage in Element 4 to the damage indicators of Elements from 5 to 7 is significantly reduced to such extent that can be comparable with that from the damage in Element 7. Therefore, the damage indicators based on the ASH flexibility can be applied for multiple damage scenarios.